УДК **531, 539.3, 539.5, 620.3**

Slyvka A.A., PhD student. 0000-0002-9173-731X;
Bilanych V.S., C.Sc., Assoc. Prof., Head of the Department of Applied Physics and Quantum Electronics. 0000-0003-4293-5675.

SIZE EFFECTS OF NANOHARDNESS IN SUPERIONIC CRYSTALS $Cu_6PS_5I(Br)$

Uzhhorod National University, 88000, Uzhhorod, 46 Pidhirna Str.,
e-mail: vitaliy.bilanych@uzhnu.edu.ua.

The mechanical properties of superionic crystals Cu_6PS_5I and Cu_6PS_5Br were studied by nanoindentation using the Continuous Stiffness Measurement (CSM) technique at room temperature. The investigations were carried out on Cu_6PS_5I and Cu_6PS_5Br single crystals grown by the vapor transport reaction method. The nanohardness (H) and Young's modulus (E) were measured using a Nano Indenter II (MTS Systems) equipped with a diamond Berkovich indenter in both pulse and harmonic load modulation modes. The parameters determined in the pulse mode were H = (3.41 ± 0.03) GPa, E = (80.47 ± 0.78) GPa for Cu_6PS_5Br and H = (3.71 ± 0.08) GPa, E = (90.33 ± 1.27) GPa for Cu_6PS_5I. A direct indentation size effect (ISE) was revealed, which was attributed to the development of plastic deformation and defect motion in the contact zone. The observed size effect was interpreted in the framework of the strain gradient plasticity (SGP) theory, which accounts for the formation of geometrically necessary dislocations beneath the indenter. The model parameters were determined as H_0 = 4.52 GPa, h* = 83 nm for Cu_6PS_5I and H_0 = 3.72 GPa, h* = 93 nm for Cu_6PS_5Br. Structural relaxation under pulsed mechanical loading was also detected. From the approximation of the relaxation curves, the plastic deformation rates (0.022 nm/s and 0.018 nm/s for Cu_6PS_5I and Cu_6PS_5Br, respectively) and the relaxation times (τ = 64 s and τ = 29 s for Cu_6PS_5I and Cu_6PS_5Br) were determined.

Keywords: superionic crystals; hardness; Young's modulus; nanoindentation; strain gradient plasticity theory.

Introduction

Crystals of Cu_6PS_5X (X = I, Br) belong to the family of argyrodite-type superionic conductors [1], which are characterized by high ionic mobility at relatively low temperatures. Due to the combination of high ionic conductivity, structural stability, and chemical inertness, these materials are considered promising solid electrolytes for applications in solid-state batteries, supercapacitors, ion-selective membranes, and other electrochemical devices [2, 3]. In addition to their practical significance, $Cu_6PS_5I(Br)$ crystals are model systems for fundamental studies of order–disorder processes, phase transitions, and structural relaxation in solids.

According to X-ray diffraction studies, Cu_6PS_5X (X = I, Br) crystals exhibit two phase transitions in the temperature range of 77–300 K. At room temperature, Cu_6PS_5I and Cu_6PS_5Br possess a cubic structure (space group $F\bar{4}3m$) [4, 5]. Upon cooling, two transitions occur: a ferroelastic one at Tc = (269 ± 2) K for Cu_6PS_5I and T_c = (268 ± 2) K for Cu_6PS_5Br, and a superionic transition at Ts = (165–175) K and T_s = (166–180) K, respectively [5]. Below the ferroelastic transition temperature, Cu_6PS_5Br crystals belong to the monoclinic symmetry (Cc), while the superionic transition is isostructural in nature [6–9].

Superionic conductivity in $Cu_6PS_5I(Br)$ compounds arises from the hopping diffusion mechanism of Cu^+ ions between energetically equivalent vacant sites under the influence of an external electric field. A high vacancy concentration and a low activation energy for ion migration determine the unique physicochemical properties of these crystals, making them valuable for designing materials with controlled ion-transport characteristics.

One of the most effective methods for studying local physicomechanical properties of crystals is

DOI: 10.24144/2414-0260.2025.2.43-54 ISSN 2414-0260

nanoindentation, which provides information about hardness (H) and Young's modulus (E) within nanoscale volumes [10–14]. It is well known that at the nanoscale, these parameters can significantly differ from their macroscopic values due to the influence of defects, inhomogeneities, and structural fluctuations. Reducing the contact area of the indenter to less than 100 nm allows experimental H and E values to approach theoretical limits and reveals effects that are not observed in conventional mechanical testing.

Special attention in such studies is given to the indentation size effect (ISE) – the dependence of the measured hardness on the indentation depth [15-19]. This phenomenon is associated with the gradient of plastic deformation and the generation of geometrically necessary dislocations (GNDs) in the contact zone. Analysis of ISE within the framework of the strain gradient plasticity (SGP) theory makes it possible to identify the mechanisms of plastic deformation initiation, determine hardening parameters, and trace the relationship between microstructure, defect subsystem, and mechanical behavior of the material [17, 18, 20-22].

The investigation of indentation size effects in Cu_6PS_5I (Br) superionic crystals is important not only for understanding the fundamental regularities of deformation and relaxation processes in ion-conducting crystals but also for improving materials for solid-state energy applications. The obtained nanomechanical characteristics can assist in optimizing the composition and structure of these compounds to enhance the stability, mechanical strength, and durability of devices based on them.

The purpose of this work is to study the nanomechanical properties of Cu_6PS_5I and Cu_6PS_5Br single crystals by nanoindentation in harmonic and pulse loading modes, and to analyze the indentation size effect (ISE) within the framework of the strain gradient plasticity model.

2. Materials and Methods

Samples and Surface Preparation.

Single crystals of Cu_6PS_5I and Cu_6PS_5Br were studied. To minimize the influence of surface roughness on the nanoindentation results, measurements were performed on the natural growth facets of the crystals. Prior to testing, the samples were cleaned in isopropanol and dried in an air stream. To avoid the overlap of plastic deformation zones from adjacent indents, the spacing between indentation points was chosen to be at least $10 \cdot a_{max}$, where a_{max} is the maximum side length of the triangular indentation imprint.

Equipment and Calibration.

Nanoindentation experiments were carried out using a Nano Indenter II (MTS Systems) equipped with a diamond Berkovich indenter (nominal apex angle equivalent to a semi-apex angle of ~65.27°). The system was operated under thermally stabilized conditions (295 ± 2 K, relative humidity 30–50%) and was equipped with high-sensitivity load and displacement sensors.

Calibration. The contact area function $A(h_c)$ was calibrated on a fused silica reference sample using the Oliver–Pharr method [23, 24], where *hc* is the contact depth. For an ideal Berkovich indenter, $A(hc) \approx 24.5\ h_c^2$; however, a polynomial correction was applied to account for the tip rounding coefficients determined from the reference sample. The system stiffness and drift error were also verified. The thermal drift was compensated by performing a pre-hold segment at a small load and/or a post-hold period after unloading.

Loading Schemes and Load–Depth (P–h) Diagrams.

Two complementary measurement protocols were applied.

1. Quasi-static P–h protocol (Oliver–Pharr method) [23].

a) Loading to the maximum load P_{max} at a constant loading rate dP/dt or at a constant nominal strain rate $d\varepsilon/dt = (1/P)(dP/dt) \approx 0.05\ s^{-1}$, where P_{max} is the peak load applied to the indenter.

b) Holding at P_{max} for 10–1000 s to separate the contributions of viscous–plastic flow (creep) and structural relaxation.

c) Unloading to 10% of P_{max} at the same dP/dt, followed by a short hold period (30–120 s) to assess drift, and then complete unloading to zero load.

The result is a complete P(h) curve consisting of three segments: loading, hold, and unloading. In the unloading segment, the initial contact stiffness $S = dP/dh$ at $P \rightarrow P_{max}$ is determined and used in the Oliver–Pharr analysis to calculate hardness and elastic modulus.

2. Harmonic modulation (CSM-type) [25, 26].

In the Continuous Stiffness Measurement (CSM) protocol, a small harmonic (sinusoidal) load component is superimposed on the primary

DOI: 10.24144/2414-0260.2025.2.43-54 ISSN 2414-0260

loading signal during the indenter penetration. This allows real-time determination of the contact stiffness at each stage of loading and provides continuous numerical values of hardness (H) and Young's modulus (E) as a function of indentation depth. To obtain continuous H(h) and E(h) profiles during linearly increasing loading, a small oscillatory force component is added:

$$P(t)=P_0(t)+P_1\sin(\omega t), \quad (1)$$

where $P_0(t)$ increases linearly, $P_1 \ll P_0$, and the oscillation frequency ω is chosen to avoid inertial artifacts. From the amplitude and phase response of the sample, the dynamic contact stiffness is determined, enabling the construction of H(h) and E(h) dependences without interrupting the loading cycle. This approach is particularly convenient for identifying and analyzing the indentation size effect (ISE) [14, 27].

For measuring the dependences H(h) and E(h), the following harmonic modulation parameters were used: the load P on the indenter was increased linearly from 0 to P_{max} = 40 mN at a loading rate of 5 mN/s, while simultaneously applying a harmonic force component P_1 with an amplitude of 0.2 mN and a frequency of 45 Hz. Thus, the resulting total load on the indenter can be expressed as:

$$P = \frac{dP}{dt} \cdot t + P_1 \cdot sin(\omega t) \quad (2)$$

where dP_0/dt = 5 mN/s; $\omega = 2\pi f$, P_1 = 0.2 mN.

In this method, the main quantities were determined according to the standard procedure:

Contact stiffness: S=dP/dh determined at the beginning of the unloading segment.

Contact depth: $h_c=h_{max}-(\varepsilon P_{max})/S$, where $\varepsilon \approx 0.75$ for a Berkovich indenter (correction for elastic recovery of the indentation).

Contact area: $A=A(h_c)$ obtained from the calibrated area function.

Hardness: $H=P_{max}/A(h_c)$.

Reduced modulus: the reduced elastic modulus (E_r), which describes the elastic interaction between the indenter and the specimen, is calculated as [23]:

$$E_r = \frac{\sqrt{\pi}}{2\beta} \cdot \frac{S}{\sqrt{A_c}} \quad (3)$$

where S = dP/dh is the contact stiffness, A_c is the projected contact area determined from the contact depth, and β is the geometric correction factor of the indenter (β ≈ 1.034 for the Berkovich indenter).

$$E_s = \frac{1-\nu_s^2}{\frac{1}{E_r}-\frac{1-\nu_i^2}{E_i}} \quad (4)$$

Young's modulus of the specimen:

where E_r is the reduced modulus of the indenter–specimen system, $E_i \approx 1140$ GPa is the Young's modulus of the diamond indenter, ν_s is the Poisson's ratio of the specimen, and $\nu_i \approx 0.07$ is the Poisson's ratio of the indenter.

Investigation of Viscoplastic Creep and Relaxation by the Quasi-Static Method

To separate the contributions of viscoplastic creep and structural relaxation, two types of holding segments were employed:

- under the peak load (P_{max}): the indentation depth h(t) was recorded for 10–1000 s. The creep rate was evaluated as dh/dt in the quasi-stationary region of the h(t) curve.
- after unloading of the indenter: the decrease in indentation depth h(t) was recorded for 30–120 s and fitted using an exponential function to determine the characteristic relaxation times.

Analysis of the Indentation Size Effect (ISE)

To analyze the ISE, hardness–depth curves H(h) were plotted and interpreted using the linearized form of the Nix–Gao model for Berkovich indentation [17]:

$$H^2 = H_0^2\sqrt{1+\frac{h^*}{h}} \quad (5)$$

where H_0 is the hardness at a depth free from strain-gradient effects, and h^* is the characteristic length associated with the density of geometrically necessary dislocations (GNDs). Within the range where the Nix–Gao law is valid, the "H^2–$1/h$" dependence is linear. Linear approximation of the experimental H(h) data according to Eq. (5) yields the intercept on the H^2 axis corresponding to H_0^2 ($h \to \infty$), while the slope of the line provides the product $H_0^2 \cdot h^*$.

3. Results and Discussion

To determine the nanohardness of the crystals, a series of 20 indentation measurements was performed, each recording a complete P–h (load–displacement) curve. The residual indentation depth (h_p) was determined from the curve and used to calculate the hardness. To evaluate Young's modulus, the initial portion of the unloading curve was analyzed, which

DOI: 10.24144/2414-0260.2025.2.43-54 ISSN 2414-0260

corresponds to a linear region representing the elastic recovery of the indentation. The Nano Indenter II software package enables automated determination of both hardness (H) and Young's modulus (E) from the load–displacement data.

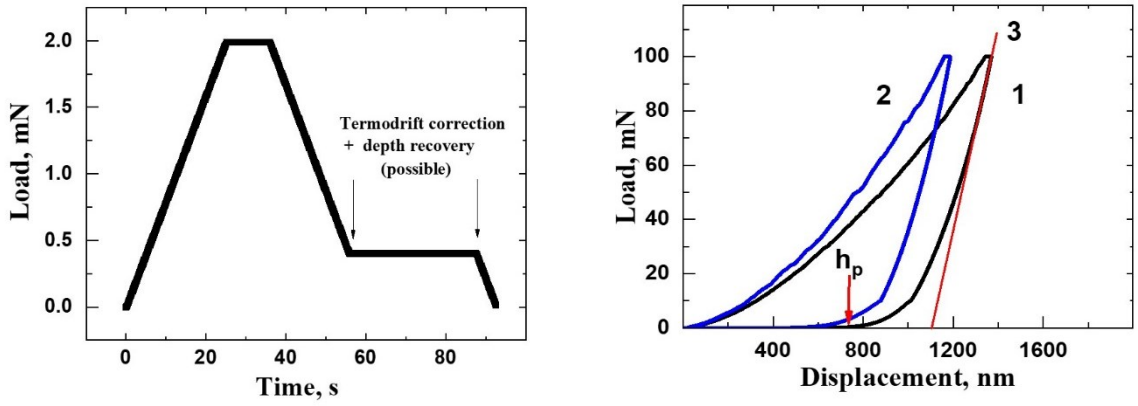

a *b*

Fig. 1. Load profile applied to the indenter (*a*) during the measurement of nanohardness and Young's modulus, and the corresponding P–h (load–displacement) curves (*b*) obtained for Cu_6PS_5Br (1) and Cu_6PS_5I (2) crystals with a holding time of 10 s at the peak load.

The averaged values of H and E for Cu_6PS_5Br and Cu_6PS_5I crystals along the (111) direction are as follows: E = (80.47 ± 0.78) GPa, H = (3.41 ± 0.03) GPa, and E = (90.33 ± 1.27) GPa, H = (3.71 ± 0.08) GPa, respectively. The mechanical characteristics of the crystals increase with the substitution of Br → I, which correlates with the higher density and lattice parameter observed in the Cu_6PS_5Br → Cu_6PS_5I series [5].

Figure 2 shows the dependences of hardness and Young's modulus of Cu_6PS_5Br and Cu_6PS_5I crystals on the penetration depth of the Berkovich indenter. These dependences were obtained in the CSM mode. In the region of h < 30 nm, the increase in E and H with increasing h may be associated with transient processes and the calibration conditions of the sharp indenter on the fused silica reference sample. The increase in E and H with increasing h is characteristic of hardness measurements performed using a spherical indenter.

The sharp Berkovich indenter used in this study possesses a finite tip radius – the so-called tip rounding radius. Therefore, at indentation depths h < 30 nm, the tip radius is comparable to the indentation depth, and the spherical geometry of the indenter makes a significant contribution to the measurement process. With increasing indentation depth (h > 30 nm), both E and H values for the studied crystals decrease over the entire range. This behavior may be attributed to the growth of deformation zones in the contact region between the indenter and the sample, their propagation deeper into the crystal, and the motion and generation of defects within the near-surface region [10]. Such a variation of E(h) and H(h) can be interpreted as a direct indentation size effect (ISE) [15, 16].

The indentation size effect (ISE) observed in crystals arises from the strain gradient of plastic deformation induced in the nanocontact region during indentation. This phenomenon can be interpreted within the framework of the Strain Gradient Plasticity (SGP) theory [17, 18]. Analysis of the dependence of nanohardness on indentation depth makes it possible to establish the correspondence between experimental data and the gradient plasticity model and to determine the characteristic parameters of this model for the studied sample. In the framework of classical plasticity theory (without strain gradients), deformation is assumed to be homogeneous throughout the material volume. Plastic flow occurs through the motion of dislocations, but the theory does not account for how these dislocations are spatially distributed. During nanoindentation, the upper layer of the material is highly deformed, while the underlying layers experience much smaller strains. Consequently, at the micro- and nanoscale, the deformation becomes nonuniform, producing a plastic strain gradient. This gradient cannot be accommodated solely by the motion of "conventional" (pre-existing or statistically stored) dislocations.

DOI: 10.24144/2414-0260.2025.2.43-54 ISSN 2414-0260

Therefore, the material necessarily generates additional dislocations to accommodate this nonuniform deformation. These additional dislocations are known as geometrically necessary dislocations (GNDs) – they do not arise from external stress but rather from deformation incompatibility within the crystal. In other words, GNDs form to "accommodate" regions of the crystal that deform differently, ensuring lattice continuity across these zones. The SGP theory accounts for the fact that the density of GNDs is proportional to the gradient of plastic strain [18].

$$\rho_{GND} \sim \frac{d\varepsilon_p}{dx} \qquad (6)$$

This means that the larger the spatial gradient of plastic deformation, the greater the number of GNDs generated and, consequently, the higher the resistance to further deformation of the material beneath the indenter—that is, the material becomes harder.

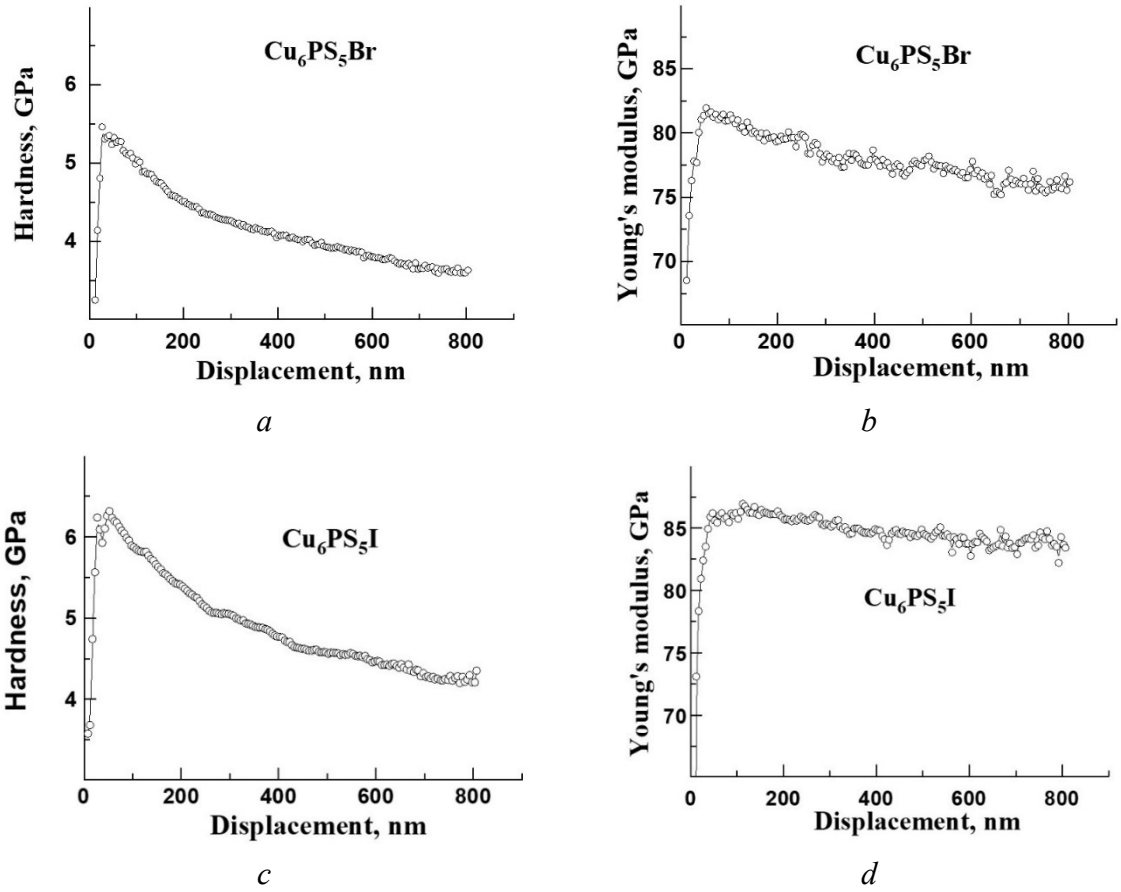

Fig. 2. Depth Dependence of Hardness and Young' modulus of single crystals Cu_6PS_5Br and Cu_6PS_5I.

As seen from Fig. 2, during nanoindentation an increase in hardness with decreasing indentation depth is observed in the region h > 30 nm. This behavior is explained by the formation of geometrically necessary dislocations (GNDs). When the contact area decreases, a strong gradient of plastic strain arises, leading to the generation of numerous GNDs, which increase the resistance to deformation and result in higher hardness. Thus, the indentation size effect (ISE) directly follows from the presence of GNDs in the contact zone between the indenter and the sample. These GNDs are responsible for material hardening at the micro- and nanoscale levels. Plastic deformation beneath the indenter occurs through dislocation motion along hemispherical slip surfaces centered at the indenter tip. Under this deformation mechanism, as the indentation size increases, the density of GNDs decreases, and dislocation movement occurs along larger slip loops. According to the SGP theory, indentation

DOI: 10.24144/2414-0260.2025.2.43-54 ISSN 2414-0260

of crystals is accompanied by the formation of circular loops of geometrically necessary dislocations with Burgers vectors perpendicular to the specimen surface [17, 18]. According to Eq. (5), H^2 should vary linearly with h^{-1}. Figure 3 presents the H(h) dependences plotted in $H^2 - h^{-1}$ coordinates for Cu_6PS_5Br (I) crystals.

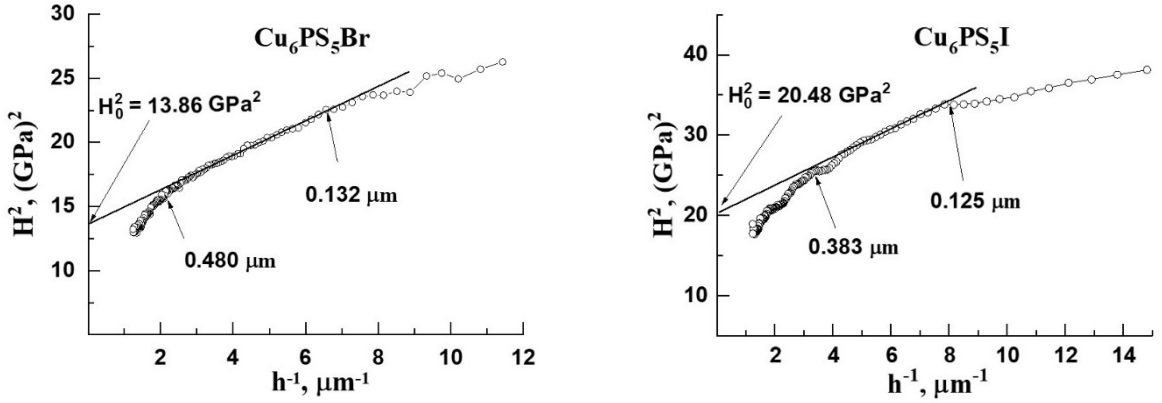

a *b*

Fig 3. The size effects approximation of *H(h)* dependence of Cu_6PS_5Br and Cu_6PS_5I single crystals in the model SGP. Show the H(h) dependence in "$\left(\frac{H^2}{H_0^2}\right)$ - h^{-1}" coordinates. (line is result of a linear approximation)

The figures show that the dependences H(h) are well approximated by a straight line according to Eq. (5), with the fitting parameters H_0 = 4.52 GPa and h^* = 83 nm for Cu_6PS_5I, and H_0 = 3.72 GPa and h^* = 93 nm for Cu_6PS_5Br. The parameter $(H_0)^2$ is determined as the intersection point of the linear region of the $H^2 = f(h^{-1})$ dependence with the ordinate axis, while $h*$ is obtained from the slope of this dependence relative to the abscissa axis. As seen from Fig. 3, the linear regions of $H^2 = f(h^{-1})$ for Cu_6PS_5I and Cu_6PS_5Br crystals are observed in the indentation depth intervals of 125 – 383 nm and 132 – 480 nm, respectively. It can be assumed that within these h intervals, a pure dislocation-controlled plastic deformation mechanism is realized, which is described by the SGP theory. At smaller indentation depths (h), deformation beneath the indenter exhibits an elasto-plastic character, while at larger depths, creep processes and crack formation may occur, indicating that the mechanical stress beneath the indenter exceeds the crystal's strength limit. Such cracks are visible in the SEM images of the indentation imprints, whereas traces of dislocation-mediated plastic deformation appear as slip bands and layer separations within the indented regions (Fig. 4).

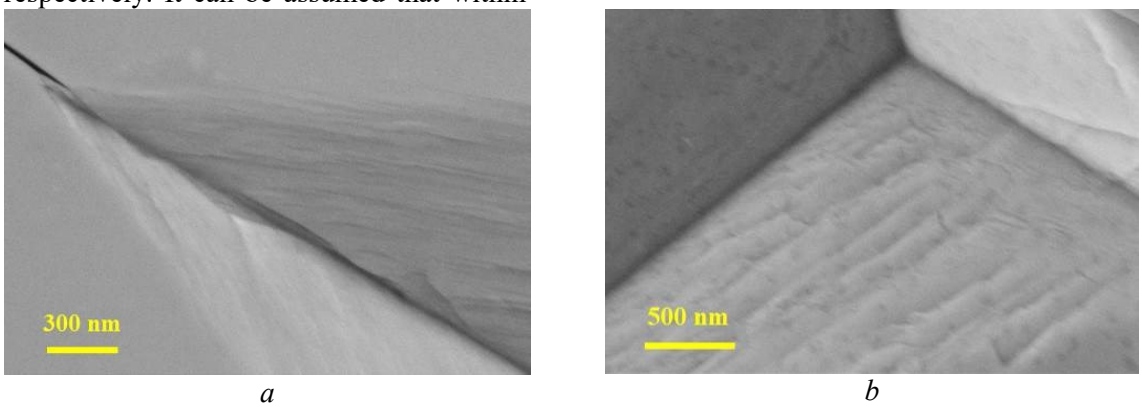

a *b*

Fig. 4. SEM images of Berkovich indenter imprints on Cu_6PS_5I (*a*) and Cu_6PS_5Br (*b*) crystals at a loading force of 50 mN.

Figure 5 presents the results of studies of Cu_6PS_5I and Cu_6PS_5Br crystals performed in the pulsed loading mode with a holding time of 900 s under load. In these measurements, the quasi-

DOI: 10.24144/2414-0260.2025.2.43-54 ISSN 2414-0260

static P–h protocol (Oliver–Pharr method) was applied, resulting in a *P(h)* curve consisting of three characteristic segments: loading (1), holding (2), and unloading (3).

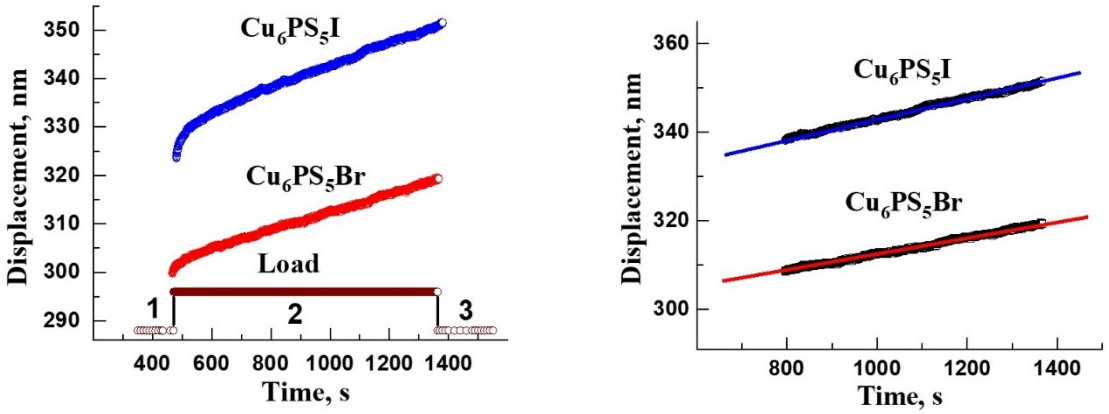

Fig. 5. Change in indentation depth during long-term holding under maximum load (*a*) and time-dependent change of indentation depth in the creep region (*b*).

The theory of elastic interaction between a rigid indenter and the plastic imprint formed at each stage of deformation is described in [28, 29]. It has been shown that the penetration of the indenter is accompanied by elastic–plastic deformation of the material beneath the indenter and in the adjacent regions. During the formation of the indentation imprint, several deformation zones are created within the contact region, which give rise to the elastic, plastic, and relaxation components of the overall deformation of the tested sample [11, 12]. The distribution of strain beneath the indenter is complex, and the total indentation depth can be expressed as the sum of contributions associated with different deformation mechanisms of the material under the indenter [12]:

$$h = h_e + h_r + h_p \qquad (7)$$

where h_e is the elastic component, $h_e = P/k$, with k being the stiffness of the material beneath the indenter and P the applied load; h_r is the relaxation (recoverable) component, $h_r = h_{r0} + h_0 \exp(-\frac{t}{\tau})$, t – where t is the loading time, (h_{ro}=h_r при $t\to\infty$), τ is the relaxation time, h_p is the plastic component; $h_p = \frac{\Delta h_p}{\Delta t} \cdot t$, $\frac{\Delta h_p}{\Delta t}$ is the viscous flow rate (creep rate).

Under a sharp indenter, several deformation zones are formed in the sample: a hydrostatic zone, a gradient zone, an elasto-plastic zone, and an elastic zone [11]. As the applied load (P) and indentation depth (*h*) increase, these zones extend deeper into the material, and their volumes expand. The relative contribution of each mechanism to the overall indentation process changes with load, leading to variations in the hardness and elastic modulus of the crystal. At smaller contact areas (under low loads), the contribution of the elastic component of deformation becomes more significant. The increase in *E* and *H* with decreasing h in the nanoregion (ISE) can be explained by the approach of the σ/E ratio to the theoretical strength limit of an ideal crystal lattice (σ ≈ 0.1E, where σ is the mechanical stress [11]).

From Fig. 5**,** it can be seen that under constant loading, the indentation depth in the crystals increases, indicating the occurrence of creep and relaxation processes. To determine the creep rate and relaxation time, the *h(t)* dependences in the interval of 500–1400 s (Fig. 5) were approximated by linear functions:

$$h(t) = (h_0 + A_0\, e^{-\frac{t}{\tau}}) + (k \cdot t + b) \qquad (8)$$

where k is the plastic deformation rate and τ is the relaxation time. The first term describes the relaxation process, while the second corresponds to the steady-state plastic deformation rate. The obtained plastic deformation rates k for Cu_6PS_5I and Cu_6PS_5Br r crystals were 0.022 nm/s and 0.018 nm/s, respectively.

DOI: 10.24144/2414-0260.2025.2.43-54 ISSN 2414-0260

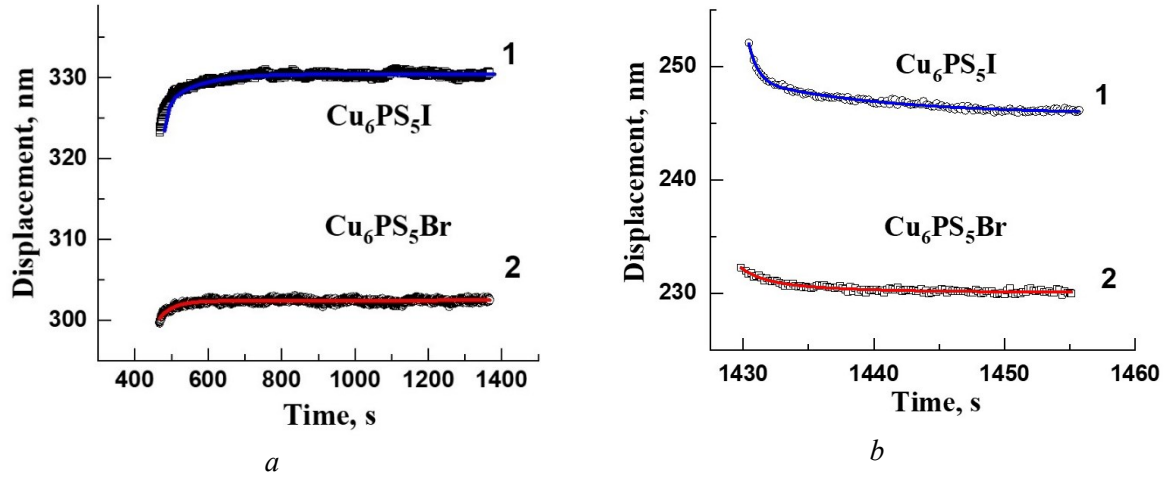

Fig. 6. Variation of indentation depth during the loading stage (a) and unloading stage (b).

To isolate the relaxation component h_r, the measured h(t) values were subtracted from the approximated linear dependence ($h_e = k \cdot t + b$). The corresponding relaxation components $h_r(t)$ are shown in Fig. 6a. These curves were fitted with exponential functions $h_r(t)$, from which the relaxation times (τ) for Cu_6PS_5I and Cu_6PS_5Br crystals were determined (see Table).

The study of the h(t) dependences after unloading of the indenter showed that, upon load removal, the indentation depth did not fully recover, indicating that the deformation of the materials contains not only plastic and elastic components but also a relaxation component. The *h(t)* dependence in this time interval was approximated using the corresponding exponential expression, and the results of the approximation are presented in Fig. 6b**.**

$$h(t) = h_0 - A_0\, e^{-\frac{t}{\tau}} \quad (9)$$

As seen from Table 1 and Fig. 6, a significant difference is observed between the Cu_6PS_5I and Cu_6PS_5Br crystals: the relaxation amplitude in Cu_6PS_5I is more than twice that in Cu_6PS_5Br, and the characteristic relaxation time is noticeably longer. This indicates a stronger and slower time-dependent response of the Cu_6PS_5I crystal under constant indentation load, whereas Cu_6PS_5Br reaches equilibrium more rapidly. Such behavior is determined by the structural and ion-transport characteristics of these crystals. In Cu_6PS_5I, the lattice parameter (a = 9.7809(6) Å) and the ionic radius of the anion I^- (R = 2.20 Å) are larger compared to those of Cu_6PS_5Br (a = 9.7236(6) Å, Br^-: R = 1.96 Å) [30].

This promotes increased disordering of the Cu^+ cation sublattice and enhances ion mobility, which activates diffusion and anelastic relaxation mechanisms. In contrast, the smaller Br^- anions in Cu_6PS_5Br form a more rigid framework that limits the rearrangement of the Cu^+ sublattice, leading to lower relaxation amplitudes and shorter relaxation times.

The recovery of the indentation imprint in Cu_6PS_5Br after unloading also occurs faster and within a smaller depth range, indicating a stiffer lattice and reduced Cu^+ ion mobility. The observed h(t) behavior after unloading confirms that the deformation response of superionic crystals contains not only an elastic component but also a significant time-dependent one, associated with ionic relaxation and diffusion processes within the Cu^+ sublattice. The prolonged post-effect (anelastic recovery) observed in Cu_6PS_5I indicates a redistribution of Cu^+ ions within the field of residual stresses and a gradual stabilization of the local structure following indentation.

Table 1. Mechanical parameters of the crystals obtained from nanoindentation measurements.

Composition	H, GPa	E, GPa	*k,* nm/s	H_0, GPa	h*, nm	τ_1, s	h_0, nm	τ_2, s
Cu_6PS_5I	3.71 ± 0.08	90.33 ± 1.27	0.022	4,52	83	65	7.5	4,4
Cu_6PS_5Br	3.41 ± 0.03	80.47 ± 0.78	0.018	3,72	93	38	2.7	3,6

DOI: 10.24144/2414-0260.2025.2.43-54 ISSN 2414-0260

Within the framework of the strain gradient plasticity (SGP) model, the Cu_6PS_5I crystal exhibits higher hardness at shallow indentation depths and a smaller characteristic length h^*, indicating more intense hardening associated with the formation of geometrically necessary dislocations (GNDs). The combination of enhanced Cu^+ ion mobility and localized stresses leads to the formation of a complex stress–strain zone beneath the indenter, the relaxation of which proceeds more slowly due to the gradual rearrangement of ionic positions. The more flexible anionic sublattice in Cu_6PS_5I also contributes to longer-lasting anelastic and ferroelastic processes, thereby increasing both the amplitude and the duration of relaxation.

Thus, the larger h_0 and τ values (Table) characteristic of Cu_6PS_5I reflect its higher structural and ionic mobility compared to Cu_6PS_5Br. This feature must be taken into account when employing such materials in solid-state electrochemical devices, where prolonged relaxation processes may influence the stability of contact interfaces and the long-term mechanical reliability of the system.

4. Conclusions

The nanomechanical properties of Cu_6PS_5I and Cu_6PS_5Br superionic single crystals were investigated using the nanoindentation method in the Continuous Stiffness Measurement (CSM) mode. It was established that the hardness and Young's modulus are H = 3.71 GPa, E = 90.3 GPa for Cu_6PS_5I and H = 3.41 GPa, E = 80.5 GPa for Cu_6PS_5Br, respectively. A direct indentation size effect (ISE) was revealed and interpreted within the framework of the strain gradient plasticity (SGP) model. The model parameters were determined as H_0 = 4.52 GPa, h^* = 83 nm for Cu_6PS_5I and H_0 = 3.72 GPa, $h*$ = 93 nm for Cu_6PS_5Br, indicating stronger hardening of the iodide crystal at shallow indentation depths. Under constant load holding, relaxation processes and viscoplastic creep were observed. For Cu_6PS_5I, the relaxation amplitude is more than twice that of Cu_6PS_5Br, and the relaxation time is significantly longer (τ = 64 s versus 29 s), indicating a stronger and slower time-dependent response in the iodide crystal, associated with higher Cu^+ ion mobility and a more flexible anionic sublattice. The analysis of h(t) behavior after unloading revealed incomplete recovery of the indentation imprint and a pronounced anelastic deformation component**.** In Cu_6PS_5I crystals, a prolonged post-effect was observed, caused by the redistribution of Cu^+ ions in the field of residual stresses and gradual stabilization of the local structure. In contrast, the recovery in Cu_6PS_5Br occurs faster, reflecting a stiffer lattice and lower ionic mobility.

Reference

1. Kuhs W.F., Nitsche R., Scheunemann K. The argyrodites – a new family of the tetrahedrally close-packed structures. *Mat. Res. Bull.* 1979, 14. 241. Doi: 10.1016/0025-5408(79)90125-9.
2. Studenyak I.P., Stefanovich V.O., Kranjčec M., Desnica D.I., Azhnyuk Yu.M., Kovacs Gy.Sh., Panko V.V. Raman scattering studies of Cu_6PS_5Hal (Hal = Cl, Br, I) fast-ion conductors. *Solid State Ionics.* 1997, 95. 221. https://doi.org/10.1016/S0167-2738(96)00477-8.
3. Nilges T., Pfitzner A. A structural differentiation of quaternary copper argyrodites: Structure-property relations of high temperature ion conductors. *Z. Kristallogr*. 2005, 220. 281. Doi: 10.5283/epub.11740.
4. Haznar A., Pietraszko A., Studenyak I.P. X-ray study of the superionic phase transition in Cu_6PS_5Br. *Solid State Ionics.* 1999, 119. 31. Doi:10.1016/S0167-2738(98)00479-2.
5. Gagor A., Pietraszko A., Drozd M., Połomska M., Pawlaczyk Cz., Kaynts D. Structural phase transitions and conduction properties of superionic, ferroelastic $Cu_6PS_5Br_{1-x}I_x$ single crystals (x = 1, 0.75, 0.5, 0.25). *J. Phys.: Condens. Matter.* 2006, 18. 4489. Doi: 10.1088/0953-8984/18/19/005.
6. Dziaugys A., Banys J., Samulionis V., Studenyak I. Dielectric Investigations of Phase Transitions in $Cu_6PS_5(I_x,Br_{1-x})$ Mixed Crystals. *Ferroelectrics*. 2011, 420. 30. Doi: 10.1080/00150193.2011.594003.
7. Samulionis V., Banys J., Studenyak I., Panko V. Ultrasonic and Piezoelectric Investigations of Phase Transitions in Ferroelastic $Cu_6PS_5(I, Br)$ Mixed Crystals. *Ferroelectrics*. 2009, 379. 62. Doi: 10.1080/00150190902850749.
8. Beeken R.B., Garbe J.J., Petersen N.R. Cation mobility in the Cu_6PS_5X (X = Cl, Br, I) argyrodites. *J. Phys. Chem. Solids.* 2003, 64. 1261. Doi: 10.1016/S0022-3697(03)00086-6.
9. Studenyak I.P., Kranjčec M., Mykailo O.A., Bilanchuk V.V., Panko V.V., Tovt V.V. Crystal growth, structural and optical parameters of $Cu_6PS_5(Br_{1-x}I_x)$ superionic conductors. *J. Optoelectron. Adv. Mater.* 2001, 3. 879.
10. Hay J., Agee P. Herbert E. Continuous stiffness measurement during instrumented indentation testing.

DOI: 10.24144/2414-0260.2025.2.43-54 ISSN 2414-0260

Exp. Tech. 2010. 34. 86. Doi: 10.1111/j.1747-1567.2010.00618.x.
11. Lucca D.A., Herrmann K., Klopfstein M.J. Nanoindentation: Measuring methods and applications. *Manuf. Technol.* 2010, 59. 803. Doi: 10.1016/j.cirp.2010.05.009.
12. Schuh C.A. Nanoindentation studies of materials. *Mater. Today*. 2006, 5. 32. Doi: 10.1016/S1369-7021(06)71495-X.
13. Li X., Zhang W., Dong Z., Wang Z., Li D., Zhang J. Study on Size Effect in Indentation Tests. *Coatings* 2022, 12(12). 1962. Doi:10.3390/coatings12121962.
14. Li X., Bhushan B. A review of nanoindentation continuous stiffness measurement technique and its applications. *Mater. Charact*. 2002, 48. 11. Doi: 10.1016/S1044-5803(02)00192-4.
15. Zong Z., Lou J., Adewoye O.O., Elmustafa A.A., Hammad F., Soboyejo W.O. Indentation Size Effects in the Nano and Microhardness of FCC Single Crystal Metals. *Mater. Manuf. Process*. 2007, 22. 228. Doi: 10.1016/j.msea.2006.06.137.
16. Milman Yu.V., Golubenko A.A., Dub S.N. Indentation size effect in nanohardness. *Acta Mater.* 2011, 59. 7480. Doi: 10.1016/j.actamat.2011.08.027.
17. Gao H., Huang Y., Nix W.D., Hutchinson J.W. Mechanism Based Strain Gradient Plasticity – I. Theory. *J.Mech. Phys. Solids*. 1999, 47. 1239. Doi: 10.1016/S0022-5096(98)00103-3.
18. Nix W. D., Gao H. Indentation Size Effects in Crystalline Materials: A Law for Strain Gradient Plasticity. *J. Mech. Phys. Solids.* 1998, 46. 411. Doi: 10.1016/S0022-5096(97)00086-0.
19. Begley M.R., Hutchinson J.W. The mechanics of size-dependent indentation. *J. Mech. Phys. Solids*. 1998, 35. 2049. Doi: 10.1016/S0022-5096(98)00018-0.
20. Asumadu T.K., Mensah-Darkwa K., Gikunoo E., Klenam D.E.P., Vandadi M., Rahbar N., Kwofie S., Soboyejo W.O. Strain gradient plasticity phenomenon in surface treated plain carbon steel. *Mater. Sci. Eng: A*. 2023, 871.144806. Doi: 10.1016/j.msea.2023.144806.
21. Ding K., Zhang Y., Birnbaum A.J., Michopoulos J.G., McDowell D. L., Zhu T. Strain gradient plasticity modeling of nanoindentation of additively manufactured stainless steel. *Extreme Mech. Lett.* 2021, 49. 101503. Doi: 10.1016/j.eml.2021.101503.
22. Mukherjee A., Banerjee B. Elastic-gap free strain gradient crystal plasticity model that effectively account for plastic slip gradient and grain boundary dissipation. *Arxiv.org.* 2024, p.1-39.
23. Oliver W.C., Pharr G.M. An improved technique for determining hardness and elastic modulus using load and displacement sensing indentation experiments. J. Mater. Res. 1992, 7. 1564. Doi: 10.1557/JMR.1992.1564.
24. Mahmoud Z. H., AL-Salman H.N.K., Kianfar E. Nanoindentation: Introduction and applications of a non-destructive analysis. *Nano TransMed*. 2024, 3. 100057. Doi: 10.1016/j.ntm.2024.100057.
25. Li X., Bhushan B. A Review of Nanoindentation Continuous Stiffness Measurement Technique and Its Applications. *Mater. Charact.* 2002, 48. 11. Doi: 10.1016/S1044-5803(02)00192-4.
26. Leitner A., Maier-Kiener V., Kiener D. Dynamic nanoindentation testing: is there an influence on a material's hardness? *Mater. Res. Lett.* 2017, 5. 486. Doi: https://doi.org/10.1080/21663831.2017.1331384
27. Shen Z., Su Y., Liang Z, Long X. Review of indentation size effect in crystalline materials: Progress, challenges and opportunities. *J. Mater. Res. Technol.* 2024, 31.117. Doi: 10.1016/j.jmrt.2024.06.071
28. Milman Yu.V., Galanov B.A., Chugunova S.I. Plasticity characteristic obtained through hardness measurement (overview No.107). *Acta metall. mater.* 1993, 41. 2523. Doi: 10.1016/0956-7151(93)90122-9.
29. Galanov B.A., Domnich V., Gogotsi Y. Elastic-plastic contact mechanics of indentations accounting for phase transformations. Exp. Mech. 2003, 43. 303. Doi: 10.1007/BF02410528.
30. Pogodin A.I., Kokhan O.P. Obtaining of Quaternary Halogenchalcogenides Cu_6PS_5Hal (Hal – I, Br) Single Crystals. *Sci. Bull. Uzhgorod Univ. (Ser. Chem.).* 2012, 27. 21. (in Ukr.).

Стаття надійшла до редакції: 30.10.2025 р.

DOI: 10.24144/2414-0260.2025.2.43-54 ISSN 2414-0260

РОЗМІРНІ ЕФЕКТИ НАНОТВЕРДОСТІ В СУПЕРІОННИХ КРИСТАЛАХ $Cu_6PS_5I(Br)$

Сливка А.А., Біланич В.С.

ДВНЗ «Ужгородський національний університет», 88000,
м. Ужгород, вул. Підгірна 46
e-mail: vitaliy.bilanych@uzhnu.edu.ua.

Досліджені механічні властивості суперіонних кристалів Cu_6PS_5I та Cu_6PS_5Br методом наноіндентування з неперервним вимірюванням жорсткості контакту (режим CSM) при кімнатній температурі. Дослідження проведені на монокристалах Cu_6PS_5I і Cu_6PS_5Br, вирощених методом газотранспортних реакцій. Вимірювання нанотвердості H і модуля Юнга E проведені на приладі Nano Indenter II (MTS Systems) з алмазним індентором Берковича в імпульсному режимі та режимі із гармонічною модуляцією навантаження на індентор. Параметри кристалів, визначені в імпульсному режимі становили H = (3,41 ± 0,03) ГПа, E = (80,47 ± 0,78) ГПа для Cu_6PS_5Br і H = (3,71 ± 0,08) ГПа, E = (90,33 ± 1,27) ГПа для Cu_6PS_5I Виявлено прямий розмірний ефект індентування (ISE), який пояснений розвитком пластичної деформації та переміщенням дефектів у приконтактній зоні. Розмірний ефект проінтерпретований у рамках теорії градієнтної пластичності деформації (Strain Gradient Plasticity, SGP), яка враховує утворення геометрично необхідних дислокацій під індентором. Визначені параметри моделі: H_0 = 4,52 ГПа, h* = 83 нм для Cu_6PS_5I і H_0 = 3,72 ГПа, h* = 93 нм для Cu_6PS_5Br. Виявлено релаксацію структури кристалів при імпульсному механічному навантаженні. Із апроксимації релаксаційних кривих визначено швидкість пластиної деформації (0,022 нм/с і 0,018 нм/с для Cu_6PS_5I і Cu_6PS_5Br) та часи релаксації (τ = 64 с і τ = 29 с для Cu_6PS_5I і Cu_6PS_5Br).

Ключові слова: суперіонні кристали; твердіть; модуль Юнга; наноіндентування; теорія градієнтної пластиної деформації.

Reference

1. Kuhs W.F., Nitsche R., Scheunemann K. The argyrodites – a new family of the tetrahedrally close-packed structures. *Mat. Res. Bull.* 1979, 14. 241. Doi: 10.1016/0025-5408(79)90125-9.
2. Studenyak I.P., Stefanovich V.O., Kranjčec M., Desnica D.I., Azhnyuk Yu.M., Kovacs Gy.Sh., Panko V.V. Raman scattering studies of Cu_6PS_5Hal (Hal = Cl, Br, I) fast-ion conductors. *Solid State Ionics.* 1997, 95. 221. https://doi.org/10.1016/S0167-2738(96)00477-8.
3. Nilges T., Pfitzner A. A structural differentiation of quaternary copper argirodites: Structure-property relations of high temperature ion conductors. *Z. Kristallogr*. 2005, 220. 281. Doi: 10.5283/epub.11740.
4. Haznar A., Pietraszko A., Studenyak I.P. X-ray study of the superionic phase transition in Cu_6PS_5Br. *Solid State Ionics.* 1999, 119. 31. Doi:10.1016/S0167-2738(98)00479-2.
5. Gagor A., Pietraszko A., Drozd M., Połomska M., Pawlaczyk Cz., Kaynts D. Structural phase transitions and conduction properties of superionic, ferroelastic $Cu_6PS_5Br_{1-x}I_x$ single crystals (x = 1, 0.75, 0.5, 0.25). *J. Phys.: Condens. Matter.* 2006, 18. 4489. Doi: 10.1088/0953-8984/18/19/005.
6. Dziaugys A., Banys J., Samulionis V., Studenyak I. Dielectric Investigations of Phase Transitions in $Cu_6PS_5(I_x,Br_{1-x})$ Mixed Crystals. *Ferroelectrics*. 2011, 420. 30. Doi: 10.1080/00150193.2011.594003.
7. Samulionis V., Banys J., Studenyak I., Panko V. Ultrasonic and Piezoelectric Investigations of Phase Transitions in Ferroelastic $Cu_6PS_5(I, Br)$ Mixed Crystals. *Ferroelectrics*. 2009, 379. 62. Doi: 10.1080/00150190902850749.
8. Beeken R.B., Garbe J.J., Petersen N.R. Cation mobility in the Cu_6PS_5X (X = Cl, Br, I) argyrodites. *J. Phys. Chem. Solids.* 2003, 64. 1261. Doi: 10.1016/S0022-3697(03)00086-6.
9. Studenyak I.P., Kranjčec M., Mykailo O.A., Bilanchuk V.V., Panko V.V., Tovt V.V. Crystal growth, structural and optical parameters of $Cu_6PS_5(Br_{1-x}I_x)$ superionic conductors. *J. Optoelectron. Adv. Mater.* 2001, 3. 879.
10. Hay J., Agee P. Herbert E. Continuous stiffness measurement during instrumented indentation testing. *Exp. Tech*. 2010. 34. 86. Doi: 10.1111/j.1747-1567.2010.00618.x.
11. Lucca D.A., Herrmann K., Klopfstein M.J. Nanoindentation: Measuring methods and applications. *Manuf. Technol.* 2010, 59. 803. Doi: 10.1016/j.cirp.2010.05.009.

DOI: 10.24144/2414-0260.2025.2.43-54 ISSN 2414-0260

12. Schuh C.A. Nanoindentation studies of materials. *Mater. Today*. 2006, 5. 32. Doi: 10.1016/S1369-7021(06)71495-X.
13. Li X., Zhang W., Dong Z., Wang Z., Li D., Zhang J. Study on Size Effect in Indentation Tests. *Coatings* 2022, 12(12). 1962. Doi:10.3390/coatings12121962.
14. Li X., Bhushan B. A review of nanoindentation continuous stiffness measurement technique and its applications. *Mater. Charact*. 2002, 48. 11. Doi: 10.1016/S1044-5803(02)00192-4.
15. Zong Z., Lou J., Adewoye O.O., Elmustafa A.A., Hammad F., Soboyejo W.O. Indentation Size Effects in the Nano and Microhardness of FCC Single Crystal Metals. *Mater. Manuf. Process*. 2007, 22. 228. Doi: 10.1016/j.msea.2006.06.137.
16. Milman Yu.V., Golubenko A.A., Dub S.N. Indentation size effect in nanohardness. *Acta Mater.* 2011, 59. 7480. Doi: 10.1016/j.actamat.2011.08.027.
17. Gao H., Huang Y., Nix W.D., Hutchinson J.W. Mechanism Based Strain Gradient Plasticity – I. Theory. *J.Mech. Phys. Solids*. 1999, 47. 1239. Doi: 10.1016/S0022-5096(98)00103-3.
18. Nix W. D., Gao H. Indentation Size Effects in Crystalline Materials: A Law for Strain Gradient Plasticity. *J. Mech. Phys. Solids.* 1998, 46. 411. Doi: 10.1016/S0022-5096(97)00086-0.
19. Begley M.R., Hutchinson J.W. The mechanics of size-dependent indentation. *J. Mech. Phys. Solids*. 1998, 35. 2049. Doi: 10.1016/S0022-5096(98)00018-0.
20. Asumadu T.K., Mensah-Darkwa K., Gikunoo E., Klenam D.E.P., Vandadi M., Rahbar N., Kwofie S., Soboyejo W.O. Strain gradient plasticity phenomenon in surface treated plain carbon steel. *Mater. Sci. Eng: A*. 2023, 871.144806. Doi: 10.1016/j.msea.2023.144806.
21. Ding K., Zhang Y., Birnbaum A.J., Michopoulos J.G., McDowell D. L., Zhu T. Strain gradient plasticity modeling of nanoindentation of additively manufactured stainless steel. *Extreme Mech. Lett.* 2021, 49. 101503. Doi: 10.1016/j.eml.2021.101503.
22. Mukherjee A., Banerjee B. Elastic-gap free strain gradient crystal plasticity model that effectively account for plastic slip gradient and grain boundary dissipation. *Arxiv.org.* 2024, p.1-39.
23. Oliver W.C., Pharr G.M. An improved technique for determining hardness and elastic modulus using load and displacement sensing indentation experiments. J. Mater. Res. 1992, 7. 1564. Doi: 10.1557/JMR.1992.1564.
24. Mahmoud Z. H., AL-Salman H.N.K., Kianfar E. Nanoindentation: Introduction and applications of a non-destructive analysis. *Nano TransMed*. 2024, 3. 100057. Doi: 10.1016/j.ntm.2024.100057.
25. Li X., Bhushan B. A Review of Nanoindentation Continuous Stiffness Measurement Technique and Its Applications. *Mater. Charact.* 2002, 48. 11. Doi: 10.1016/S1044-5803(02)00192-4.
26. Leitner A., Maier-Kiener V., Kiener D. Dynamic nanoindentation testing: is there an influence on a material's hardness? *Mater. Res. Lett.* 2017, 5. 486. Doi: https://doi.org/10.1080/21663831.2017.1331384
27. Shen Z., Su Y., Liang Z, Long X. Review of indentation size effect in crystalline materials: Progress, challenges and opportunities. *J. Mater. Res. Technol.* 2024, 31.117. Doi: 10.1016/j.jmrt.2024.06.071
28. Milman Yu.V., Galanov B.A., Chugunova S.I. Plasticity characteristic obtained through hardness measurement (overview No.107). *Acta metall. mater.* 1993, 41. 2523. Doi: 10.1016/0956-7151(93)90122-9.
29. Galanov B.A., Domnich V., Gogotsi Y. Elastic-plastic contact mechanics of indentations accounting for phase transformations. Exp. Mech. 2003, 43. 303. Doi: 10.1007/BF02410528.
30. Погодін А.І., Кохан О.П. Одержання монокристалів тетрарних галогенхалькогенідів Купруму Cu_6PS_5Hal (Hal – I, Br). *Науковий вісник Ужгородського університету. Сер.: Хімія.* 2012, 27. 21. (in Ukr.).

DOI: 10.24144/2414-0260.2025.2.43-54 ISSN 2414-0260